



Deposited via The University of York.

White Rose Research Online URL for this paper:

<https://eprints.whiterose.ac.uk/id/eprint/186915/>

Version: Published Version

---

**Article:**

Xu, Xufeng, Ong, Quy, Mao, Ting et al. (2022) Experimental method to distinguish between a solution and a suspension. *Advanced materials interfaces*. 2200600. ISSN: 2196-7350

<https://doi.org/10.1002/admi.202200600>

---

**Reuse**

This article is distributed under the terms of the Creative Commons Attribution-NonCommercial (CC BY-NC) licence. This licence allows you to remix, tweak, and build upon this work non-commercially, and any new works must also acknowledge the authors and be non-commercial. You don't have to license any derivative works on the same terms. More information and the full terms of the licence here:

<https://creativecommons.org/licenses/>

**Takedown**

If you consider content in White Rose Research Online to be in breach of UK law, please notify us by emailing [eprints@whiterose.ac.uk](mailto:eprints@whiterose.ac.uk) including the URL of the record and the reason for the withdrawal request.

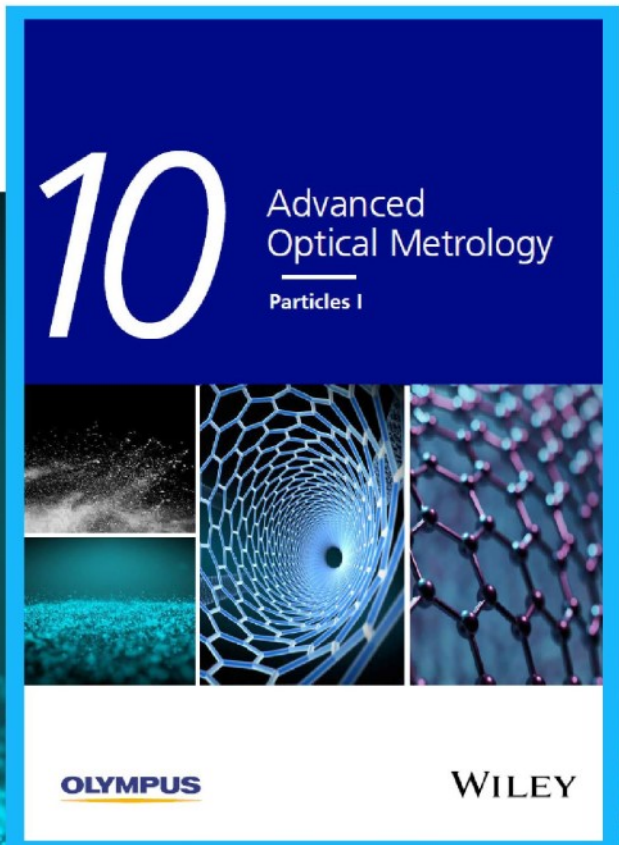


# Particles I

Access the latest eBook →

Particles: Unique Properties,  
Uncountable Applications

**Read the latest eBook and  
better your knowledge with  
highlights from the recent  
studies on the design and  
characterization of micro-  
and nanoparticles for  
different application areas.**



**Access Now**

This eBook is sponsored by

**OLYMPUS**

**WILEY**

# Experimental Method to Distinguish between a Solution and a Suspension

Xufeng Xu, Quy Ong, Ting Mao, Paulo Jacob Silva, Seishi Shimizu, Luca Rebecchi, Ilka Kriegel, and Francesco Stellacci\*

Dispersion of objects in a fluid phase can be classified as solutions (Gibbs free energy of mixing,  $\Delta G_{\text{mix}} < 0$ ) or suspensions ( $\Delta G_{\text{mix}} > 0$ ) depending on their thermodynamic stability. Small objects tend to form solutions, larger ones suspensions, e.g., molecules versus micrometer-sized colloids. Proteins and nanomaterials fall between these two size regimes. The long-standing issue of whether proteins and nanoparticles are dissolved or suspended remains an important research question. Here, a simple, versatile, and experimentally robust method, based on sedimentation equilibrium analytical ultracentrifugation (SE-AUC), which can determine whether proteins, nanoparticles, or polymers form solutions or suspensions, is presented. SE-AUC determines the osmotic pressure profile for a dispersion. Such a profile for solutions (equilibrium one-phase systems) is independent of the initial and the operating conditions. The opposite is true for suspensions that are non-equilibrium two-phase systems. This study proves that bovine serum albumin and lysozyme form solutions while ferritin and apoferritin form suspensions.

## 1. Introduction

Solutions<sup>[1,2]</sup> are one-phase systems that form spontaneously<sup>[3]</sup> (negative Gibbs free energy of mixing,  $\Delta G_{\text{mix}} < 0$ ) while suspensions<sup>[4,5]</sup> are two-phase systems that are metastable<sup>[6]</sup> ( $\Delta G_{\text{mix}} > 0$ ). Equilibrium properties of solutions<sup>[7,8]</sup> obey equilibrium thermodynamics.<sup>[9]</sup> Suspensions have been successfully explained by Derjaguin–Landau–Verwey–Overbeek (DLVO) theory,<sup>[8,10]</sup> that, however, can also be trivially modified to model some solutions.<sup>[2,4,5,11]</sup> Given that the free energy of mixing ( $\Delta G_{\text{mix}}$ ) is the key driving force to form a solution, calorimetry has been widely used to measure accurately the thermodynamic quantities involved with mixing molecules in solvents. Slow sedimentation provides an easy way to visualize the relative instability in a suspension system.<sup>[12]</sup> However, distinguishing between a solution and a suspension becomes very complex for nanometer-scale objects, such as nanoparticles as well as biomacromolecules, especially proteins. The calorimetric signature is often too small to be realistically measurable, and equally the sedimentation time for dispersions becomes years, hence observing it is experimentally unreasonable (e.g., because other phenomena such as degradation can occur). Therefore, determining univocally whether dispersions of objects with characteristic sizes in the nanometer scale form solutions or suspensions remains an open research question. This is particularly important for nanomaterials and proteins.

There is a significant body of literature on the topic. Bergin et al.<sup>[13]</sup> used scanning probe microscopies to demonstrate that carbon nanotubes (CNTs) can spontaneously exfoliate upon dilution. This could indicate that CNTs are in solution, but it is always hard to rule out the effect of thermal energy. Lin et al.<sup>[14]</sup> used dynamic light scattering to determine the reversibility in the thermally driven dissolution/precipitation cycle in gold nanoparticles (AuNPs). They found the process to be fully reversible with temperature<sup>[15]</sup> and concluded that their AuNPs were in solution. A laser scattering method was also employed by Yang et al. to measure the solubility of CdSe–stearates nanocrystal–ligands complex.<sup>[16]</sup> The reproducible and fully reversible temperature-driven sharp turbidity change (within  $\pm 1$  K) indicated that their particles were in solution. Centrone et al.<sup>[17]</sup> used the optical density measurements to determine uniquely the saturation concentration of their AuNPs. This measurement also implies that the particles were in solution. Doblas et al.<sup>[18]</sup>

There is a significant body of literature on the topic. Bergin et al.<sup>[13]</sup> used scanning probe microscopies to demonstrate that carbon nanotubes (CNTs) can spontaneously exfoliate upon dilution. This could indicate that CNTs are in solution, but it is always hard to rule out the effect of thermal energy. Lin et al.<sup>[14]</sup> used dynamic light scattering to determine the reversibility in the thermally driven dissolution/precipitation cycle in gold nanoparticles (AuNPs). They found the process to be fully reversible with temperature<sup>[15]</sup> and concluded that their AuNPs were in solution. A laser scattering method was also employed by Yang et al. to measure the solubility of CdSe–stearates nanocrystal–ligands complex.<sup>[16]</sup> The reproducible and fully reversible temperature-driven sharp turbidity change (within  $\pm 1$  K) indicated that their particles were in solution. Centrone et al.<sup>[17]</sup> used the optical density measurements to determine uniquely the saturation concentration of their AuNPs. This measurement also implies that the particles were in solution. Doblas et al.<sup>[18]</sup>


X. Xu, Q. Ong, T. Mao, P. J. Silva, F. Stellacci  
Institute of Materials  
Ecole Polytechnique Fédérale de Lausanne (EPFL)  
Lausanne 1015, Switzerland  
E-mail: francesco.stellacci@epfl.ch

S. Shimizu  
York Structural Biology Laboratory  
Department of Chemistry  
University of York  
Heslington, York YO10 5DD, UK

L. Rebecchi, I. Kriegel  
Functional Nanosystems  
Istituto Italiano di Tecnologia (IIT)  
via Morego 30, Genova 16163, Italy

L. Rebecchi  
Dipartimento di Chimica e Chimica Industriale  
Università degli Studi di Genova  
Genova 16146, Italy

F. Stellacci  
Bioengineering Institute  
Ecole Polytechnique Fédérale de Lausanne (EPFL)  
Lausanne 1015, Switzerland

 The ORCID identification number(s) for the author(s) of this article can be found under <https://doi.org/10.1002/admi.202200600>.

© 2022 The Authors. Advanced Materials Interfaces published by Wiley-VCH GmbH. This is an open access article under the terms of the Creative Commons Attribution-NonCommercial License, which permits use, distribution and reproduction in any medium, provided the original work is properly cited and is not used for commercial purposes.

DOI: 10.1002/admi.202200600

measured the agglomeration fraction of AuNPs in different organic solvents during the evaporation process, using small angle X-ray scattering (SAXS). For their particles they found a varying saturation concentration, thereby concluding that their particles were in suspension. All these methods are valid but they are very specific to the system studied and hard to generalize to all the nanoscale objects that need to be studied.

There are also theoretical papers to determine key differences between solutions and suspensions. Shimizu thoroughly discussed different general thermodynamic stability conditions to judge whether one system is in solution or in suspension.<sup>[12]</sup> A very detailed calculation of  $\Delta G_{\text{mix}}$  was also demonstrated by Wheeler et al.<sup>[19]</sup> to justify the solution of boronated silicon nanoparticles in dimethyl sulfoxide (DMSO) by using a statistical thermodynamic theoretical model. However, there is still not a conclusive and experimental-robust method to determine the thermodynamic status of a dispersion for a wide range of systems. In this paper, we present a simple and universal experimental method to address this long-standing question. We use sedimentation equilibrium analytical ultracentrifugation (SE-AUC).<sup>[20,21]</sup> It has been established that osmotic pressure  $\Pi$  versus number density  $\rho$  can be obtained<sup>[22]</sup> using the SE-AUC experiments.<sup>[21]</sup> Indeed, using the equation of state [EOS, Equation (1)], SE-AUC is commonly used to determine  $B_2$  and  $B_3$  the second and third virial coefficients in solution ( $kT$  is the product of the Boltzmann constant by the temperature).

$$\frac{\Pi}{kT} = \rho + B_2\rho^2 + B_3\rho^3 + \dots \quad (1)$$

The key concept in our work is that a solution is a one-phase equilibrium system, hence reaching a specific thermodynamic state for a solution, i.e., varying concentration, temperature, or pressure, has to be path-independent.<sup>[7,9]</sup> This implies that the EOS plots for a solution, determined using SE-AUC from varying initial or operating conditions, must be all equivalent. In other words, one must be able to reduce all EOS plots into a single master curve that has to be independent of the sample history (i.e., sedimentation parameters, including the angular velocity of a centrifugal field and the initial loading concentration of a sample). In contrast, a suspension is in a two-phase thermodynamically metastable state that typically will tend to form irreversible aggregates. For suspensions, EOS plots cannot obey the principle of path-independence as the formation of aggregates will depend on the initial or operating conditions and change the osmotic pressure of the system. Hence, we postulate that performing SE-AUC experiments at varying initial and operating condition will distinguish univocally between the two cases as solution will produce EOS plots that will collapse into a single master curve. Suspensions will have curves that start from a single curve (all dispersions are solutions at concentrations low enough to allow for entropy to dominate, namely, the ideal condition) but then diverge into separate curves depending on the initial or operating conditions. The concept is illustrated in **Figure 1**.

Experimentally, we first prepare samples at varying initial concentrations. We have tried to cover the largest possible concentration range within the instrumental limitations of AUC. These samples are loaded into the ultracentrifuge and the instrument is run to achieve sedimentation-diffusion equilibrium

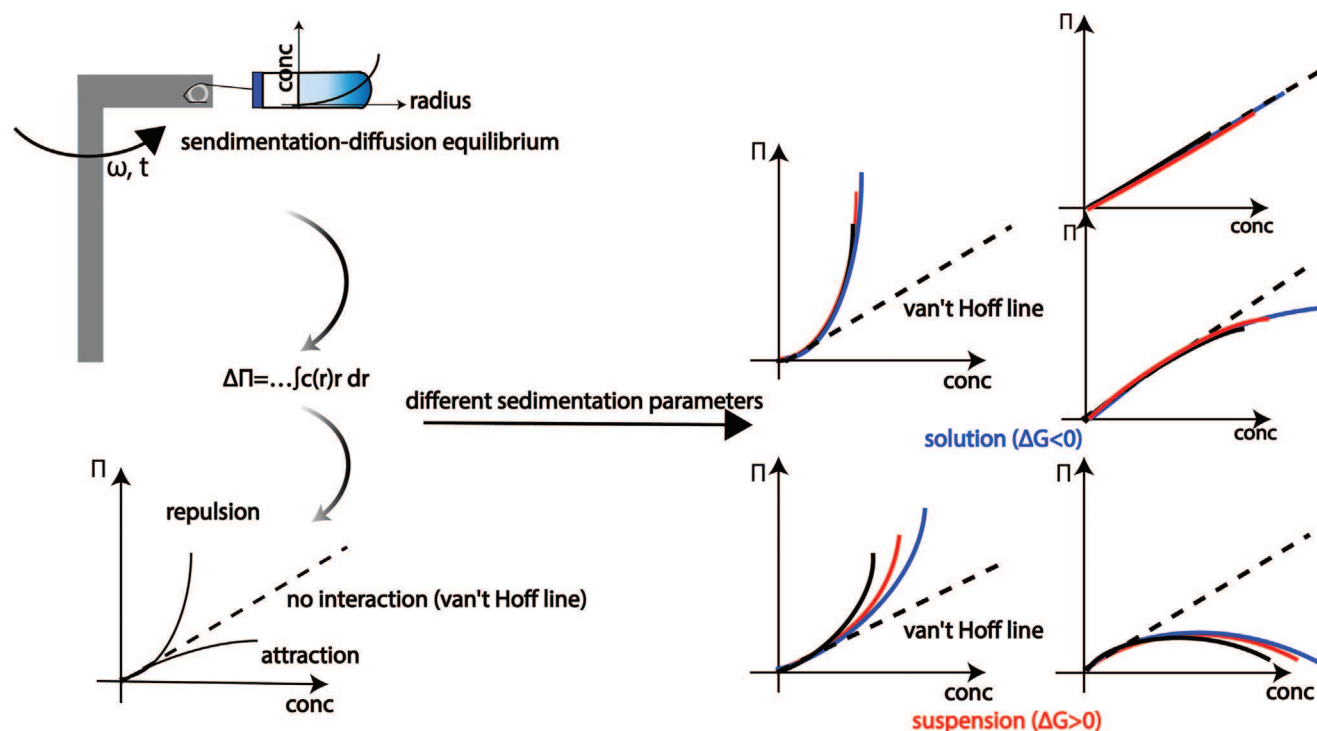


**Figure 1.** Schematic illustration of our experimental method. The dispersion of objects can result in a solution ( $\Delta G_{\text{mix}} < 0$ ) or a suspension ( $\Delta G_{\text{mix}} > 0$ ). In our method, samples are loaded into an analytical ultracentrifuge for sedimentation-diffusion equilibrium. Then, the osmotic pressure ( $\Pi$ ) can be calculated by integrating concentration [Equation (2)] and plotted versus concentration, which is calculated as number density ( $\rho$ ). Finally, we verify whether the plots follow a master curve in different sedimentation parameters, such as the angular velocity of a centrifugal field and the initial loading concentration of a sample. If so, it is a solution otherwise it is a suspension.

libria at several different angular velocities. The concentration profiles (stable over time) that form in the cells are converted into equilibrium osmotic pressure profiles using the well-known relation<sup>[23]</sup> [Equation (2)]

$$\Delta\Pi = \omega^2 \left( \frac{\partial d}{\partial c} \right)_{\mu} \int_{r_m}^{r_1} c(r) r dr \quad (2)$$

where  $c$  the mass concentration of the solute species,  $\omega$  the angular velocity,  $d$  the density, and  $r$  the radial position (where  $r_m$  the sample meniscus position and  $r_1$  the cell bottom position). Equation (2) allows all EOS plots for different sedimentation parameters (initial concentration  $c_i$  and angular velocity  $\omega$ ) to be collapsed into a single master curve. When this is possible, we conclude that we have a solution otherwise we must conclude that we are in presence of a suspension. Obviously, the state of a dispersion depends on concentration (free energy is concentration dependent), and the conclusions that can be made with this method apply only to the concentration range that is experimentally accessible. This and other limitations of this method are discussed thoroughly in the last part of the article.

## 2. Results and Discussion

To verify the strategy, a typical suspension of polystyrene nanoparticles (PS NPs) of diameter = 60 nm in water was prepared with the addition of  $15 \times 10^{-3}$  M sodium chloride (NaCl), which allows suppressing the charge redistribution due to the Donnan effect<sup>[24]</sup> (size distribution by dynamic light scattering is shown in Figure S1, Supporting Information). The PS NPs dispersion of  $17 \text{ mg mL}^{-1}$  was loaded into the ultracentrifuge and the sedimentation-diffusion equilibria were reached at different speeds (2500, 3000, and 3500 rpm).<sup>[25,26]</sup> The EOS plots for different angular velocities were then calculated and plotted, as shown in Figure 2a. At a lower number density than  $\approx 1\text{E}20 \text{ m}^{-3}$  (conc =  $10 \text{ mg mL}^{-1}$ ), the EOS are all collapsed in a single master curve indicating solution behavior. Furthermore, at those concentration the master curve is very close to the line that is expected for an ideal solution (shown as the dashed line in Figure 2a) as it follows van't Hoff equation ( $\frac{\Pi}{kT} = \rho$ ). At a higher number density, the three curves diverge, indicating that at those concentrations the dispersions are suspensions.

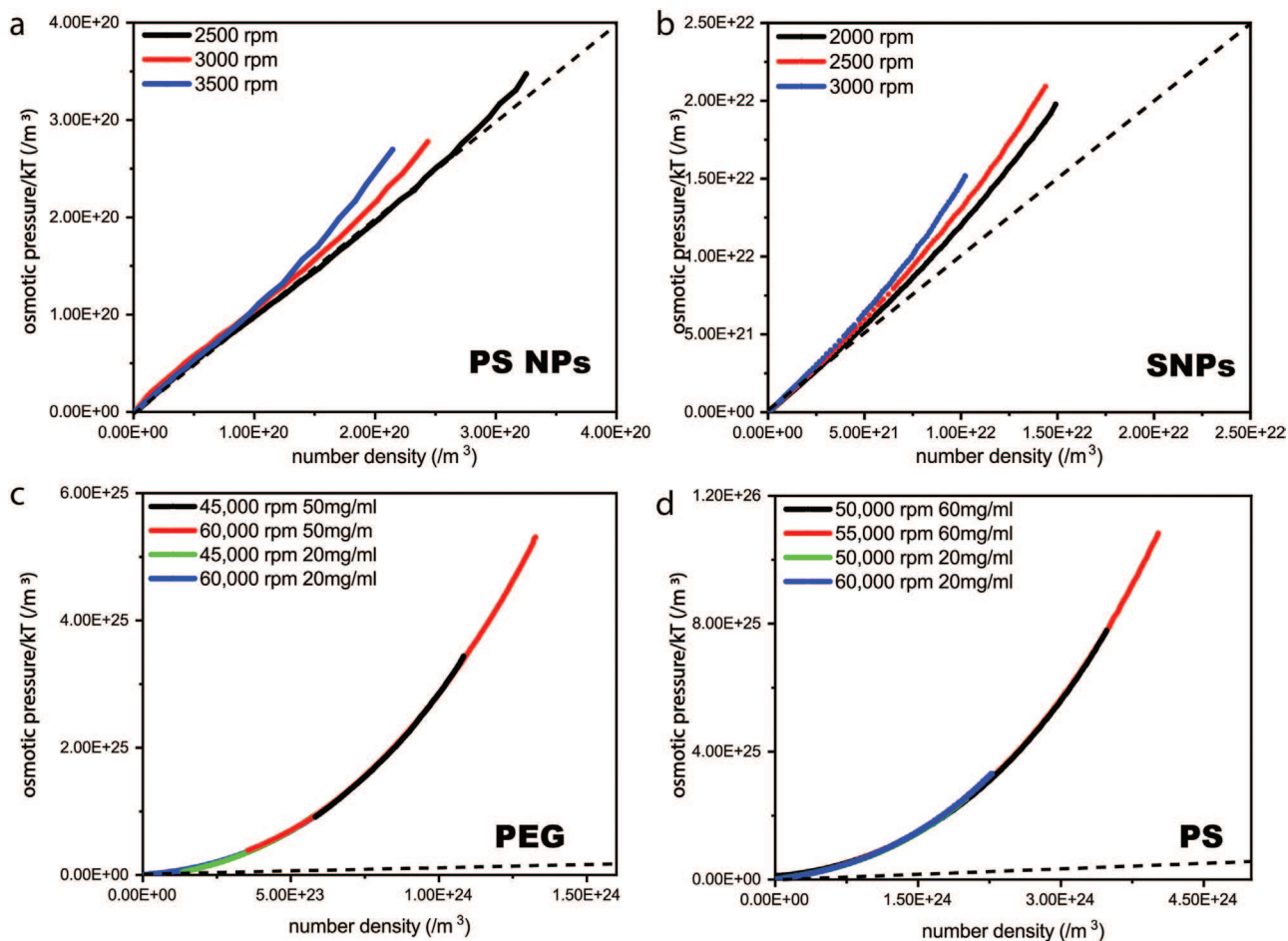


**Figure 2.** Osmotic pressure versus number density in SE-AUC experiments for a) PS NPs of  $17 \text{ mg mL}^{-1}$  in water at different angular velocities (2500, 3000, and 3500 rpm); b) SNPs of  $15 \text{ mg mL}^{-1}$  in water at different angular velocities (2000, 2500, and 3000 rpm); c) PEG (35 000 Da) of 50 and 20  $\text{mg mL}^{-1}$  in water at different angular velocities (60 000 and 45 000 rpm); d) PS (30 000 Da) of 60 and 20  $\text{mg mL}^{-1}$  in toluene at different angular velocities (60 000 and 50 000 rpm). Because PEG (35 000 Da) is still too light in an ultracentrifugal field, the meniscus is not depleted yet even at the highest accessible speed (60 000 rpm) in the AUC instrument. In this case, all the curves were vertically shifted to demonstrate the master curve, as described in details by Stanley and Strey.<sup>[27]</sup>

The fact that the EOS are above ideal line indicates a system dominated by particles repulsion, in full agreement with the DLVO theory. Very similar observations are made for a typical suspension of silica nanoparticles (SNPs) of 20 nm in diameter in water. The nanoparticles behave as in suspension when the concentration exceeds the ideal concentration ( $\approx 1\text{E}21\text{ m}^{-3}$  or  $6\text{ mg mL}^{-1}$ ), as shown in Figure 2b. We also found that EOS diverged when the initial concentration was varied but the divergence is not as large as that for varying angular velocities, as shown in Figure S2 (Supporting Information).

By contrast, we tested two systems that have been established to form solutions. We first studied polyethylene glycol (PEG, Mw = 35 000 Da) in water. We varied the initial loading concentration (20 and 50  $\text{mg mL}^{-1}$ ) as well as the angular velocity (45 000 and 60 000 rpm). As shown in Figure 2c the EOS obtained for this system collapse in a single master curve. Similarly, we studied polystyrene (PS, Mw = 30 000 Da) in toluene. We varied both initial loading concentration (20 and 60  $\text{mg mL}^{-1}$ ) and angular velocity (50 000 and 60 000 rpm). As shown in Figure 2d a single master curve encompasses all the EOS. To verify that both the instrumental and experimental noise do not play a major role when comparing EOS curves, we performed multiple measurements of the same sample. In one case we measured three times the same sample, in another we three replicates of a measurement always using a different solution, albeit coming from the same stock. The former case is shown in Figure S3a,b (Supporting Information), revealing a signal to noise ratio of  $<1\%$  at concentration above  $2 \times 10^{23}\text{ m}^{-3}$ , i.e., in the region of interest. The noise increases at very low concentrations as expected in AUC, but only goes to 7%. In the latter case, the signal/noise ratio was found to be  $\approx 3\%$ , as shown in Figure S3c,d (Supporting Information). Therefore, deviations of EOS like the ones shown in this paper can be

safely attributed to differences in the curves and not to noise effects.

We then moved on to prove that our method could be used to determine the nature of nanoparticle dispersions. We started by investigating 11-mercapto-1-undecanesulphonate capped gold nanoparticles<sup>[28]</sup> (MUS-Au NPs) in  $150 \times 10^{-3}\text{ M NaCl}$  (average core diameter 3.1 nm, TEM image shown in Figure S4, Supporting Information). We found that all EOS plots collapsed into a single master curve regardless of angular velocities (Figure 3a) and initial loading concentrations (Figure 3b) until the highest accessible concentration for the absorbance optics in our AUC ( $\approx 8\text{E}22\text{ m}^{-3}$  or  $60\text{ mg mL}^{-1}$ ). This indicated that they form solutions in water. We should point out that the EOS indicate a nearly ideal solution for these particles, we believe that this is the case because at  $150 \times 10^{-3}\text{ M NaCl}$  the charge repulsion is basically screened for these particles. To test this hypothesis and to determine whether this screening is needed to have a solution, we repeated the measurements at a lower ionic strength ( $15 \times 10^{-3}\text{ M NaCl}$ ). As shown in Figure 3c the EOS become nonideal and repulsive but they still collapse into a single master curve. We then tested indium-tin-oxide nanoparticles (ITO NPs)<sup>[29]</sup> in hexane (average core diameter 8.8 nm, TEM image is shown in Figure S5, Supporting Information). A dispersion of  $20\text{ mg mL}^{-1}$  ITO NPs in hexane was loaded into the ultracentrifuge and three different angular velocities of 2000, 2500, and 3500 rpm were applied. As shown in Figure 3d, the EOS plot has the signature of a suspension system with an ideal region that stops at  $\approx 2\text{E}21\text{ m}^{-3}$  or  $8\text{ mg mL}^{-1}$ .

A strong indication of the power of this technique comes from the analysis of PEG-coated AuNPs. These particles are composed of a gold core of 5.4 nm in average (TEM image is shown in Figure S6, Supporting Information) coated with PEG

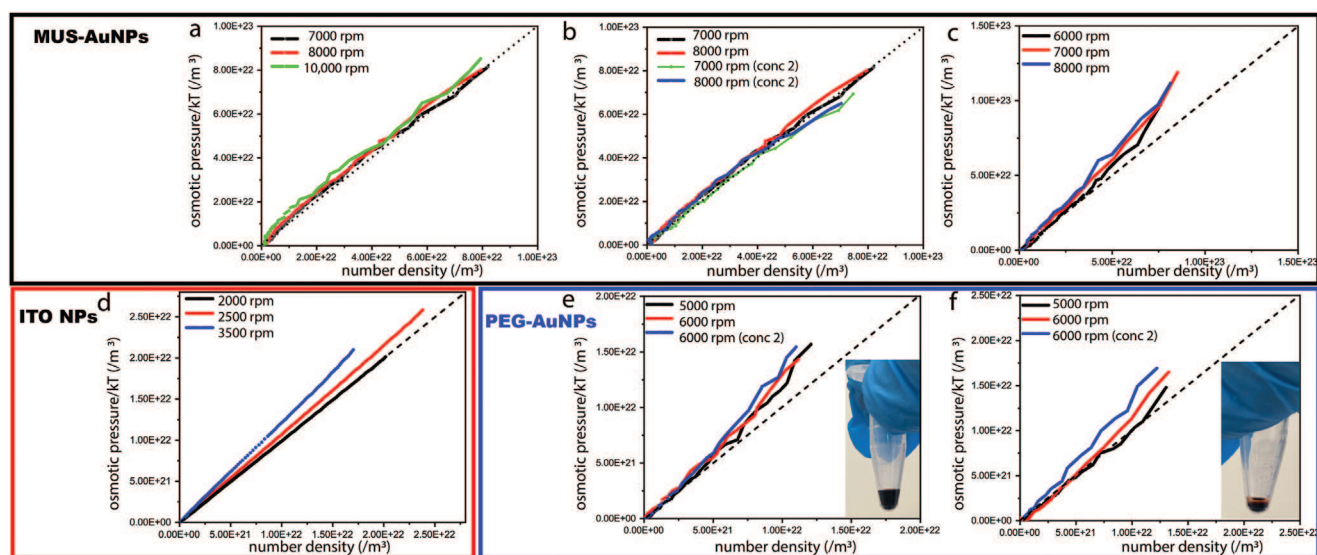


**Figure 3.** Osmotic pressure versus number density in SE-AUC experiments for a,b) MUS-Au NPs of  $10\text{ mg mL}^{-1}$  in water (with  $150 \times 10^{-3}\text{ M NaCl}$ ) where a) at different angular velocities (7000, 8000, and 10 000 rpm) and b) at different initial concentrations (10 and  $2.5\text{ mg mL}^{-1}$ ) in water (with  $15 \times 10^{-3}\text{ M NaCl}$ ) at different angular velocities (6000, 7000, and 8000 rpm); c) MUS-Au NPs of  $10\text{ mg mL}^{-1}$  in water (with  $15 \times 10^{-3}\text{ M NaCl}$ ) at different angular velocities (2000, 2500, and 3500 rpm); d) ITO NPs of  $20\text{ mg mL}^{-1}$  in water at different angular velocities (2000, 2500, and 3500 rpm); e) PEG-AuNPs where e) in water at different concentrations and angular velocities (5000 and 6000 rpm at  $10\text{ mg mL}^{-1}$ , 6000 rpm at  $30\text{ mg mL}^{-1}$ ) and f) in  $0.5\text{ M K}_2\text{CO}_3$  at different concentrations and angular velocities (5000 and 6000 rpm at  $5\text{ mg mL}^{-1}$ , 6000 rpm at  $10\text{ mg mL}^{-1}$ ). The insets show  $25\text{ mg mL}^{-1}$  PEG-AuNPs in water (e) and  $0.5\text{ M K}_2\text{CO}_3$  (f) after one heating ( $70^\circ\text{C}$ ) and cooling cycle (room temperature).

( $M_w = 2000$  Da). These particles were studied in water under two conditions, one in deionized (DI) water the other in  $0.5$  M  $K_2CO_3$ . The latter case was chosen because similar systems tend to aggregate in such conditions.<sup>[30]</sup> We studied the particles in the two cases with cryo-electron tomography (cryo-ET)<sup>[31]</sup> and SAXS. As shown in Figure S7 (Supporting Information), the particles did not show significant difference when studied with these two techniques. By contrast, we observed different behavior when studying them with SE-AUC. Concentrated PEG-AuNPs in DI water at different conditions (angular velocities: 5000 and 6000 rpm; loading concentrations: 10 and 30 mg mL<sup>-1</sup>) followed one master curve, as shown in Figure 3e. However, after the addition of  $0.5$  M  $K_2CO_3$ , a single master curve could not be found anymore (angular velocities: 5000 and 6000 rpm; loading concentrations: 5 and 10 mg mL<sup>-1</sup>), as shown in Figure 3f. Hence, the conclusion of the AUC studies is that these particles are in solution in DI water but are in suspension in  $0.5$  M  $K_2CO_3$ , despite their spatial distribution in water being practically the same in those two cases (as shown by cryo-ET and SAXS in Figure S7, Supporting Information). This example represents the power of the technique that we propose here. We have also confirmed the AUC finding with a temperature cycling experiment. After a heating (to 70 °C) and cooling cycle (to room temperature), PEG-AuNPs at 25 mg mL<sup>-1</sup> in water stayed homogenous while PEG-AuNPs at the same concentration with  $0.5$  M  $K_2CO_3$  precipitated towards the thermodynamically stable phase-separated state, as shown in the insets of Figure 3e,f.

Now, we turned our attention to proteins. Highly concentrated model protein dispersions of bovine serum albumin (BSA) in phosphate-buffered saline (PBS, pH 7.4) were prepared. Two samples at 100 and 40 mg mL<sup>-1</sup> were loaded into the AUC cells and the sedimentation-diffusion equilibria were reached at three different angular velocities of 28 000, 32 000, and 35 000 rpm, respectively. The results are shown in Figure 4a,b. The EOS plots follow one master curve, independent of angular velocities and loading concentrations. Thus, in concentration range from 0 to  $\approx 4E23$  m<sup>-3</sup> (50 mg mL<sup>-1</sup>), BSA in PBS behaves as in solution. We then studied lysozyme in the same buffer. Two samples at 10 and 40 mg mL<sup>-1</sup> were loaded into the ultracentrifuge and the sedimentation-diffusion equilibria were reached at three different angular velocities of 45 000, 48 000, and 52 000 rpm, respectively. The master curve can also be found in the number density ranges from 0 to  $\approx 2E24$  m<sup>-3</sup> (50 mg mL<sup>-1</sup>) for lysozyme, as shown in Figure 4c,d, which proves that lysozyme in PBS behaves as in solution.

Given the results discussed above, one would be tempted to conclude that proteins always form solutions. We found that this is not the case. To demonstrate this, we studied ferritin and apoferritin. Ferritin in saline solutions (purchased from Sigma) as well as apoferritin in PBS, prepared with the initial concentration = 5 mg mL<sup>-1</sup> were both found to behave as a suspension, as no master curve was present beyond the ideal concentration, as shown in Figure 4e,f.

We can now discuss the limitations of this approach. Firstly, the high-spatial-resolution interference optics embedded in the ultracentrifuge does not work properly for plasmonic nanoparticles, due to significant light absorption at incident light wave-

length (675 nm). As a result, we have lower spatial-resolution UV-vis absorbance optics. In this case, more noisy EOS plots cannot be avoided as illustrated in this paper in the case of AuNPs (Figure 3) that contrast with the smooth data plots for all the other samples in our study where interference optics could be used. We expect that the problem would be more evident for larger plasmonic particles that absorb more. Secondly, the highest accessible sample concentration depends on the limit of the detection systems. For the UV-vis absorbance optics, the maximum OD to be analyzed can only reach  $\approx 1$  because it is the linearity limit in the Beer-Lambert law. However, a capillary cell setup<sup>[23,26]</sup> (the light pathlength down to  $\approx 1$  mm compared to 1.5 and 3 cm of the shortest standard AUC cells) can be used to compensate it. For the interference optics, the reachable concentration range is much wider than absorbance optics but incident light can be steered away from the detector due to a steep concentration gradient, resulting in signal disappearance. This effect gets more severe when the angular velocity ramps up. Thirdly, these experiments are time-consuming,  $\approx 1$  d for a typical SE-AUC experiment at 1 angular velocity. Reducing the total sample size is a strategy that could be used to shorten the equilibrium time.<sup>[32]</sup> Lastly, the temperature range is limited to 4–40 °C because of AUC instrumental limitations. Angular velocity range is also limited. The instrumental range is 1100–60 000 rpm for SE-AUC experiments, but each sample limits the range even more. The reason is that a significant change of osmotic pressure is required for proper EOS curves, which depends very much on the molecular mass of samples. Especially a depleted meniscus is needed so that the zero osmotic pressure is identified in order to calculate the absolute value of osmotic pressure for EOS curves. This determines the minimum working angular velocity. On the other hand, the maximum working angular velocity shall not induce a too steep concentration gradient, which steers away the incident light and induces signal disappearance. A complete or nearly complete sedimentation of sample also needs to be avoided due to a limited amount of data points. These all limits the angular velocity range available when this method is employed.

### 3. Conclusion

In conclusions, we demonstrated a facile experimental method to distinguish between a suspension and a solution. The method is based on plotting the EOS curves derived from SE-AUC experiments at varying operating and starting conditions. We have shown that for solutions, EOS curves all fall onto a single master curve, while the opposite is true for suspensions. The method is based on the principle of path-independence for a thermodynamically stable system and demonstrated successful applications in a range of different systems including polymers, nanoparticles, and proteins. We have shown that nanoparticles can go from solution to suspension by simple addition of a salt. We have also found that some proteins (BSA and lysozyme) are in solution while others (ferritin and apoferritin) are in suspension. This method may provide deeper understanding on proteins properties in water, for example, their driving force toward phase separation, a key step for organelle formation.

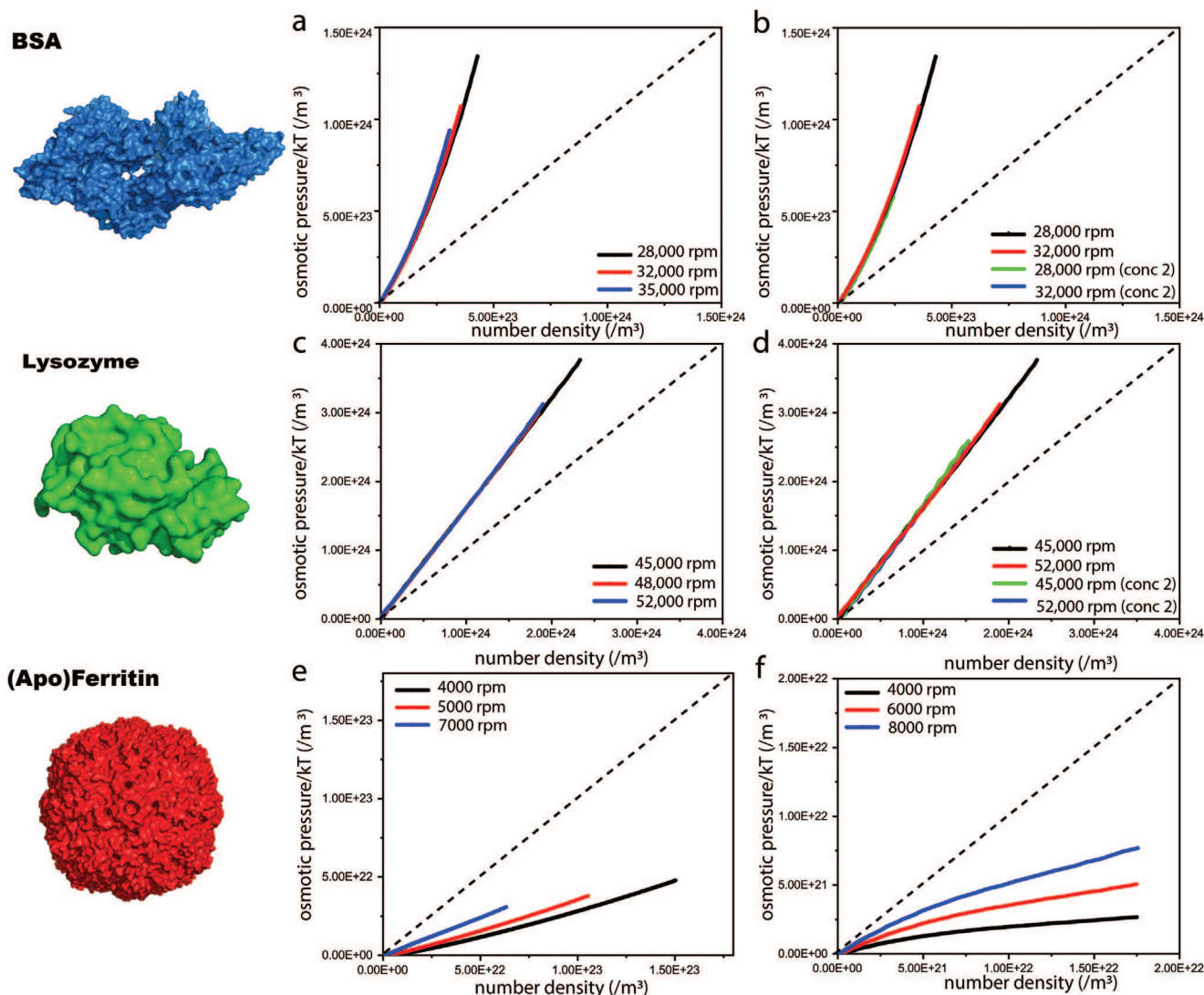


**Figure 4.** Osmotic pressure versus number density in SE-AUC experiments for BSA in phosphate-buffered saline (PBS, pH 7.4) at a) different angular velocities (28 000, 32 000, and 35 000 rpm) and b) different concentrations (100 and 40 mg mL<sup>-1</sup>) in SE-AUC experiments; lysozyme in PBS (1x, pH 7.4) at c) different concentrations (10 and 40 mg mL<sup>-1</sup>) and d) different angular velocities (45 000, 48 000, and 52 000 rpm); e) ferritin in saline at different angular velocities (4000, 5000, and 7000 rpm) and f) apoferritin (5 mg mL<sup>-1</sup>) in PBS (pH 7.4) at different angular velocities (5000, 6000, and 8000 rpm). All the three protein structures (4F5S, 6LYZ, and 6PXM) were reproduced under the CC0 1.0 license from the RCSB PDB.<sup>[36–38]</sup>

## 4. Experimental Section

**Materials:** The silica nanoparticles were purchased from nanoComposix. The polyethylene glycol (Mw = 35 000 Da), polystyrene (Mw = 30 000 Da), PEG-coated gold nanoparticles, bovine serum albumin, lysozyme, and ferritin in saline solutions were all purchased from Sigma-Aldrich. Apoferritin was purchased from Lucerna Chem AG.

**Sedimentation-Diffusion Equilibrium Experimental Procedures:** In a typical SE-AUC experiment, an analytical ultracentrifuge (Beckman Coulter ProteomeLab XL-I/XL-A) with titanium double sector cells of 1.5 mm/3 mm pathlength was used. For highly absorbing gold nanoparticles, home-made capillary cells<sup>[23,26]</sup> of ≈0.1 mm pathlength were used. An appropriate amount (e.g., 12 μL for a 1.5 mm cell) of highly concentrated sample was added into the sample cell by a syringe. At last, SE-AUC experiments were performed at 20 °C with scan intervals of 3 h using interference and absorbance optics (radial steps: 1 μm). Typically, a sedimentation-diffusion equilibrium was reached after 24 h. It is verified when concentration profiles stay unchanged for at least 10 h. The effect of solvent compressibility was not considered because even in the extreme

case of the organic solvent (toluene) at the highest speed (60 000 rpm), the density change ( $\kappa = 9 \times 10^{-10} \text{ Pa}^{-1}$ ) was estimated to be 0.6% between the base (7.1 cm) and the meniscus (6.7 cm) of the cell. Therefore, the solvent compressibility hardly affected the solvent density and thus the effect of solvent compressibility on osmotic pressure is negligible. The density of toluene was estimated by the following equation

$$d_r = d_m \left[ 1 + \kappa d_m \omega^2 (r^2 - m^2) / 2 \right] \quad (3)$$

where  $d_r$  and  $d_m$  are the solvent densities at radial position  $r$  and meniscus, respectively;  $\kappa$  is the compressibility;  $r$  is the radial position; and  $m$  is the meniscus position.

**EOS Curve Plotting:** The concentration gradient curves (raw data from SE-AUC experiments) were converted to an EOS plot (osmotic pressure  $\Pi$  vs number density  $\rho$ ) by using Equations (4) and (5)<sup>[23,33]</sup> where  $\rho$  is the number density of the solute species,  $\omega$  is the angular velocity,  $m$  is the buoyant mass of the particles,  $N_A$  is the Avogadro number,  $M$  is the molecular weight, and  $d_s$  is solvent density. The concentration can

be either calculated from absorbance data by knowing the extinction coefficients or from interference data by knowing the specific refractive index increment<sup>[34,35]</sup>

$$\Delta\Pi = \omega^2 m \int_{r_m}^{r_i} \rho(r) r dr, \quad (4)$$

and

$$\rho = \frac{cd_s N_A}{M} \quad (5)$$

## Supporting Information

Supporting Information is available from the Wiley Online Library or from the author.

## Acknowledgements

X.X. and F.S. acknowledge the support of European Union's Horizon 2020 Research and Innovation program under Grant Agreement No. 101017821 (LIGHT-CAP). I.K. and L.R. acknowledge the support of both European Union's Horizon 2020 European Research Council, under Grant Agreement No. 850875 (Light-DYNAMO) and European Union's Horizon 2020 Research and Innovation program under Grant Agreement No. 101017821 (LIGHT-CAP).

Open access funding provided by Ecole Polytechnique Federale de Lausanne.

## Conflict of Interest

The authors declare no conflict of interest.

## Data Availability Statement

The data that support the findings of this study are openly available in Zenodo with <https://doi.org/10.5281/zenodo.6552819>.

## Keywords

nanoparticles, proteins, sedimentation equilibrium analytical ultracentrifugation, solution, suspension, thermodynamics

Received: March 16, 2022

Revised: April 27, 2022

Published online:

- [1] C. M. Dobson, *Semin. Cell Dev. Biol.* **2004**, *15*, 3.  
 [2] J. Zhang, in *Protein-Protein Interactions-Computational and Experimental Tools*, **2012**, Ch. 18.  
 [3] T. L. Hill, *An Introduction to Statistical Thermodynamics*, Dover Publications, Inc., New York **1986**.  
 [4] D. N. Petsev, B. R. Thomas, S.-T. Yau, P. G. Vekilov, *Biophys. J.* **2000**, *78*, 2060.  
 [5] G. Pellicane, D. Costa, C. Caccamo, *J. Phys.: Condens. Matter* **2003**, *15*, 375.  
 [6] K. S. Birdi, *Handbook of Surface and Colloid Chemistry*, CRC Press, Boca Raton, FL **2008**.

- [7] K. G. Denbigh, *The Principles of Chemical Equilibrium: With Applications in Chemistry and Chemical Engineering*, Cambridge University Press, Cambridge **1981**.  
 [8] W. B. Russel, W. Russel, D. A. Saville, W. R. Schowalter, *Colloidal Dispersions*, Cambridge University Press, Cambridge **1991**.  
 [9] R. H. Fowler, *Statistical Thermodynamics*, CUP Archive, **1939**.  
 [10] B. V. Derjaguin, N. V. Churaev, V. M. Muller, *Surface Forces*, Springer US, Boston, MA **1987**, pp. 293–310.  
 [11] D. Leckband, S. Sivasankar, *Colloids Surf., B* **1999**, *14*, 83.  
 [12] S. Shimizu, N. Matubayasi, *J. Colloid Interface Sci.* **2020**.  
 [13] S. D. Bergin, V. Nicolosi, P. V. Streich, S. Giordani, Z. Sun, A. H. Windle, P. Ryan, N. P. P. Niraj, Z. T. Wang, L. Carpenter, *Adv. Mater.* **2008**, *20*, 1876.  
 [14] X. Lin, G. Wang, C. Sorensen, K. Klabunde, *J. Phys. Chem. B* **1999**, *103*, 5488.  
 [15] J. Powell, R. Schwieters, K. Bayliff, E. Herman, N. Hotvedt, J. Changstrom, A. Chakrabarti, C. Sorensen, *RSC Adv.* **2016**, *6*, 70638.  
 [16] Y. Yang, H. Qin, M. Jiang, L. Lin, T. Fu, X. Dai, Z. Zhang, Y. Niu, H. Cao, Y. Jin, F. Zhao, X. Peng, *Nano Lett.* **2016**, *16*, 2133.  
 [17] A. Centrone, E. Penzo, M. Sharma, J. W. Myerson, A. M. Jackson, N. Marzari, F. Stellacci, *Proc. Natl. Acad. Sci.* **2008**, *105*, 9886.  
 [18] D. Doblas, T. Kister, M. Cano-Bonilla, L. González-García, T. Kraus, *Nano Lett.* **2019**, *19*, 5246.  
 [19] L. M. Wheeler, N. J. Kramer, U. R. Kortshagen, *Nano Lett.* **2018**, *18*, 1888.  
 [20] T. Laue, W. Stafford III, *Annu. Rev. Biophys. Biomol. Struct.* **1999**, *28*, 75.  
 [21] T. M. Laue, *Methods in Enzymology*, Elsevier, Amsterdam **1995**, pp. 427–452.  
 [22] A. Vrij, R. Tuinier, in *Structure of Concentrated Colloidal Dispersions Fundamentals of Colloids and Interface Science*, Vol. IV, (Ed: J. Lyklema), Elsevier, Amsterdam **2005**.  
 [23] M. G. Page, T. Zemb, M. Dubois, H. Cölfen, *ChemPhysChem* **2008**, *9*, 882.  
 [24] A. P. Philippe, *J. Phys.: Condens. Matter* **2004**, *16*, S4051.  
 [25] X. Xu, H. Cölfen, *Nanomaterials* **2021**, *11*, 333.  
 [26] X. Xu, T. Franke, K. Schilling, N. A. J. M. Sommerdijk, H. Cölfen, *Nano Lett.* **2019**, *19*, 1136.  
 [27] C. B. Stanley, H. H. Strey, *Macromolecules* **2003**, *36*, 6888.  
 [28] A. Verma, O. Uzun, Y. Hu, Y. Hu, H. S. Han, N. Watson, S. Chen, D. J. Irvine, F. Stellacci, *Nat. Mater.* **2008**, *7*, 588.  
 [29] A. Agrawal, I. Kriegel, E. L. Runnerstrom, F. Scotognella, A. Llordes, D. J. Milliron, *ACS Photonics* **2018**, *5*, 2044.  
 [30] N. I. Anaraki, M. Liebi, Q. Ong, C. Blanchet, A. K. Maurya, F. Stellacci, S. Salentinig, P. Wick, A. Neels, *Adv. Funct. Mater.* **2022**, *32*, 2110253.  
 [31] Q. Ong, T. Mao, N. I. Anaraki, Ł. Richter, C. Malinverni, X. Xu, F. Olgiati, P. H. J. Silva, A. Murello, A. Neels, D. Demurtas, S. Shimizu, F. Stellacci, M. Horiz, **2022**, *9*, 303.  
 [32] D. G. Rhodes, R. E. Bossio, T. M. Laue, in *Guide to Protein Purification*, 2nd ed. (Eds: R. R. Burgess, M. P. Deutscher), Academic, San Diego, CA **2009**, pp. 691–723.  
 [33] J. van Rijssel, V. F. Peters, J. D. Meeldijk, R. J. Kortschot, R. J. van Dijk-Moes, A. V. Petukhov, B. H. Erne, A. P. Philippe, *J. Phys. Chem. B* **2014**, *118*, 11000.  
 [34] W. Maechtle, L. Börger, *Analytical Ultracentrifugation of Polymers and Nanoparticles*, Springer, Berlin **2006**.  
 [35] J. L. Cole, *Analytical Ultracentrifugation*, Academic, San Diego, CA **2015**.  
 [36] A. Bujacz, *Acta Crystallogr., Sect. D: Biol. Crystallogr.* **2012**, *68*, 1278.  
 [37] R. Diamond, *J. Mol. Biol.* **1974**, *82*, 371.  
 [38] M. Kopylov, K. Kelley, L. Y. Yen, W. J. Rice, E. T. Eng, B. Carragher, C. S. Potter, *National Institutes of Health/National Human Genome Research Institute (NIH/NHGRI)* **2019**, Horse spleen apoferritin light chain, <https://doi.org/10.2210/pdb6PXM/pdb>.